Electronic structure of K_2NiF_4

L. Sangaletti
Dipartimento di Fisica, "A. Volta" dell'Università, via A. Bassi, 6, 27100 Pavia, Italy

F. Parmigiani
Laboratori del Centro Informazioni, Studi ed Esperienze, Tecnologie Innovative S.p.A., Materials Division, P. O. Box 12081, 20134 Milano, Italy
and Facoltà di Scienze, Università di Como, Como, Italy

E. Ratner and Z.-X. Shen
Department of Applied Physics, Stanford University, Stanford, California, 94305

C. Chemelli
Laboratori del Centro Informazioni, Studi ed Esperienze, Tecnologie Innovative S.p.A., Materials Division, P. O. Box 12081, 20134 Milano, Italy

O. Jepsen
Max-Planck-Institute for Solid State Research, D-7000 Stuttgart 80, Federal Republic of Germany
(Received 19 July 1993; revised manuscript received 19 January 1994)

An experimental and theoretical study of the electronic structure of K_2NiF_4 is presented. Core-level and valence-band x-ray angle-integrated photoemission experiments are reported and the data analyzed through a configuration-interaction impurity-cluster model. The charge transfer and the Mott-Hubbard charge fluctuations are studied and the energies involved estimated. The effect of these mechanisms on the spectral structures is identified. The comparison of local-density-functional band calculations with angle-resolved photoemission experiments shows significant discrepancies. This demonstrates that electron-correlation effects are indeed important and one-electron band-structure calculations are inadequate to describe this compound.

I. INTRODUCTION

Electronic correlations in $3d$ transition-metal (TM) compounds have been widely investigated by core-level x-ray photoelectron spectroscopy (XPS).[1-4] The results have pointed out the role of the charge transfer Δ as well as the d-d repulsive Coulomb U_{dd} energies in determining the shape of core-level XP spectra. In this context, the impurity-cluster configuration interaction approach to the Anderson Hamiltonian has been used to estimate Δ and U_{dd} and their trend both in compounds with the same metal ion and different ligand (i.e., Cu and Ni halides) (Refs. 1,2) and in compounds with the same ligand and different metal ions (i.e., $3d$ TM's oxides).[3] The effects of electronic correlations can also be evinced through an analysis of band structure, comparing the experimental data obtained from angle-resolved ultraviolet photoelectron spectroscopy (ARUPS) experiments to density-functional band-structure calculations.[5,6]

This paper reports a study of K_2NiF_4 layered perovskite, performed by means of different electron spectroscopies (XPS, UPS, ARUPS, resonant photoemission spectroscopy, RESPES, and constant initial-state spectroscopy, CIS). Transition-metal compounds A_2MF_4 (A=K, Rb; M=Mn, Fe, Co, Ni, Cu, Zn) are ionic crystals with halide-perovskite layered structure. They crystallize in the D_{4h}^{17} tetragonal space group in the paramagnetic phase. Crystals of these compounds consists of successive MF_2 planes, separated by two AF planes. Alternatively, the crystal structure can be viewed as a two-dimensional network of transition metal–halogen octahedra, piling up in the crystallographic c direction. These compounds are generally regarded as good examples of two-dimensional Ising antiferromagnets and several experiments were performed in order to study their magnetic properties.[7-10]

To the best of our knowledge, very few experimental data are available about A_2MF_4 electronic structure (see, e.g., Ref. [11] and references therein). As regards K_2NiF_4, the unit cell dimensions are $a=b=4.006$ Å and $c=13.076$ Å. The Néel temperature is 97.1° (Ref. 7) and the energy gap is greater than 6.5 eV, as indicated by optical data.[11]

The study of the K_2NiF_4 electronic structure by means of photoelectron spectroscopies is important for several reasons. First of all, K_2NiF_4 have the same crystal structure as La_2CuO_4 oxygen perovskite, the precursor compound of the first high-T_c superconductor, and it could be important to study charge fluctuations in such a system. Moreover, Ni-F coordination in K_2NiF_4 is similar to Ni-O coordination in NiO. This fact suggests a comparative study of the electronic properties of the two compounds focusing the discussion on the role of ligand

0163-1829/94/50(24)/17854(13)/$06.00

(O, F) in shaping the UP and XP spectra and in determining the strength of the electronic correlations. Within this framework, the effect of covalence and hybridization degree of the M^{2+}-ligand bond on the electronic structure could be evidenced.

The discussion about experimental results is based on two issues.

(1) Electronic correlations in valence-band spectra, as well as in core-level spectra, are evidenced by satellite features. An estimate of the degree of correlation can be obtained when these features are unambiguously identified and correctly attributed.

(2) Further information about correlation effects can be obtained through a comparison between the measured and the calculated band dispersion. Although the band calculations have well-known problems in describing these materials, such comparison still leads to new insights about them. In particular, this may help to know to what extent it is possible to borrow the results from a N electron system to describe the excited state of a $N-1$ electron system.

The present study represents also a contribution to the debate on the adequacy of single-electron band theory to describe band structures where both localized, less dispersed, and nonlocalized, more dispersed, electronic states coexist.[5,6,12–14] This is the case of TM compounds such as NiO, CoO, high temperature superconducting cuprates and K_2NiF_4, where the electronic structure is characterized by the interplay between $3d$ TM electrons and ligand $2p$ electrons. Localized and nonlocalized electronic states can interact both through bond hybridization, which is related to metal-ligand distance in the crystal structure, and through charge fluctuations of the charge-transfer type. In our case, a comparison of K_2NiF_4 with NiO allows us to evaluate the effects of metal-ligand bond electronegativity on electronic correlations.

The paper is organized as follows. The description of the experimental and computational details are reported in Sec. II. The experimental results, core-level data, and angle-integrated valence band XPS data, including the results of a fitting based on an impurity-cluster configuration-interaction model, are described in Sec. III, Sec. IV A, and Sec. IV B, respectively. Angle-resolved valence band UPS data and the comparison with LDA band-structure calculations are shown and discussed in Sec. IV C. Section V reports the conclusions.

II. EXPERIMENTAL AND COMPUTATIONAL DETAILS

K_2NiF_4 single crystals were grown by the flux method, under argon/H_2 atmosphere using a mixture of KF and 35 mol% $KNiF_3$ at a cooling rate of 1 °C h^{-1}. Once grown, the single crystals, several millimeters in size, were controlled by Laue reflection.[11]

The XPS spectrometer was a Perkin-Elmer Model 5400 with a monochromatic Al $K\alpha$ source having a 200×650 μm^2 spot size. The pass energy of the analyzer was set to 5.85 eV, which gave an ultimate energy resolution of 0.35 eV, as measured on the Ag$3d_{5/2}$ core line. Binding energies (BE) were determined by reference to the Fermi edge of Ag, where the Ag $3d_{3/2}$ core level was set to 368±0.1 eV.

Synchrotron radiation from the SPEAR storage ring, available at the beam line 1–2 of the SSRL Stanford Synchrotron facility was used to perform ARUPS, CIS, and RESPES measurements in the valence-band energy range. The radiation was dispersed by means of a TGM 6-m monochromator. This system is equipped with three interchangeable gratings, of which the 823 1/mm, working in the 25–90-eV range, was used. The UPS spectrometer was a VG ADES 400 equipped with a hemispherical analyzer (angular resolution ±2°). The pass energy of the analyzer was set to give an ultimate energy resolution of 0.5 eV, as measured on Au Fermi edge. Even better resolution was tried, but that did not enhance our ability to resolve the details of the valence band.

To reduce surface charging an electron flood gun was used during UPS and XPS runs. The energy of the electron beam was adjusted in order to minimize the width of the F $1s$ core line and it resulted at about 2 eV. This procedure allows us to reduce the surface charging. However, this procedure does not exclude effects of nonuniform or nonradial electric fields which in turn could affect the k vector of the outgoing photoelectrons.

Binding energies were measured with reference to the K $3p$ BE, which was set at 18.4 eV. The samples were cleaved in UHV at a pressure of 2×10^{-10} torr and the pressure inside the chamber during the experiments was better than 3×10^{-10} torr. The fracture surface was identified as the ⟨001⟩ surface. The samples were prepared for ARUPS measurements orienting their surface through Laue analysis.

It was not possible to control the quality of the cleaved surface using an *in situ* low-energy electron diffraction since a high energy from the primary electron beam was required to obtain some signal. To avoid possible damages due to high-energy electrons, the surface orientation was controlled only through Laue transmission analysis. Therefore, it is not possible to exclude the presence of stacking faults that could affect the surface quality.

Because the K_2NiF_4 energy bands were not available in literature, they had to be calculated. First-principles density-functional band-structure calculations using the local potential of von Barth and Hedin[15] (LDA) were carried out. To this purpose, the calculations were performed by the scalar-relativistic self-consistent linear-muffin-tin-orbital method of Andersen in the atomic-spheres approximation including the combined correction term and with a minimal basis set in the standard way.[16,17] Both nonspin polarized and spin-polarized band-structure calculations were performed. Like in NiO, the non-spin-polarized bands do not have a gap, whereas, a gap of ≈0.5 eV was found for the spin-polarized case, in agreement with the insulating nature of the compound. For this reason the latter calculations were chosen to be compared with the experimental results. A detailed LDA calculation for K_2NiF_4 has recently appeared and reference to this are included in Ref. 18.

III. RESULTS

Figure 1 reports the F 1*s* XP spectrum of K_2NiF_4. The binding energy is 684.4 eV and the full width at half maximum is 2.1 eV. The line shape is symmetric and no satellites on the high BE side are present. This result suggests that inside the crystal volume sampled by the XP probe and within the resolution of the present experiment, fluorine ions are present in a single oxidation state. Satellite structures around the F 1*s* core line were not detected even for a binding-energy range larger than that reported in Fig. 1. However, this region has not been investigated in detail and, therefore, we cannot exclude the presence of very low intensity structure.

In Fig. 2, the Ni 2*p* XPS spectrum is reported. Two groups of structures, separated by nearly 17 eV can be detected. The group at lower BE is attributed to the Ni $2p_{3/2}$ contribution, while the group at higher BE to the Ni $2p_{1/2}$ contribution. Focusing on the Ni $2p_{3/2}$ structures, a main line at 852 eV, a satellite at 858 eV, and a low-intensity structure at 863 eV can be observed. The spectral structures are similar to the ones observed in highly correlated TM compounds as NiO and Ni halides.[2,3]

The origin of the low-intensity structure observed at about 843.0 eV is obscure. Such a line has never been detected in the Ni $2p_{3/2}$ region of NiO. It is possible to exclude that this emission is due to an artifact such as unidentified satellite lines of the Al $k\alpha$ source, being the spectrum obtained with a monochromatic line, or to contaminants which have to be excluded on the basis of a 0–1000-eV survey spectrum. A further ambiguity about the origin of this line arises from the presence of the *F* KLL Auger emission at about 830 eV. A deeper investigation exceeds the aim of the present work.

The K 2*p* XP spectrum is reported in Fig. 3. The photoemitted K 2*p* electrons originate a spin-orbit split structure with a low BE peak at 293 eV and a high BE peak at 296 eV. No evidence of satellite structures is observed.

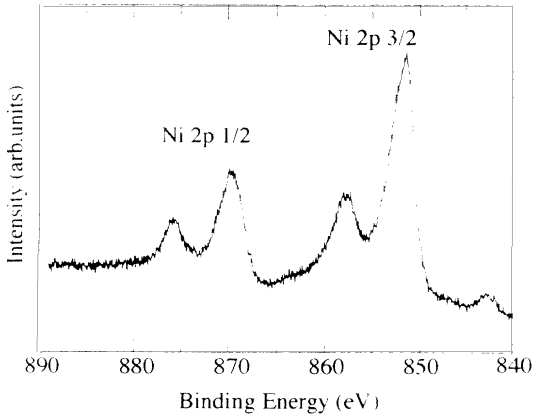

FIG. 2. Ni 2*p* core-level XP spectrum for K_2NiF_4.

Figure 4 reports XPS (Al $k\alpha$) and UPS ($h\nu=66$ eV) spectra of K_2NiF_4 valence band. The XPS spectrum shows a peak (*A*) at 5 eV followed by a structure (*B*) extending from 6 to 11 eV with the maximum at 8.0 eV. A further spectral line (*C*) can be observed at 13 eV. Finally, the variation of spectrum slope at 4 eV, points out a structure (*D*) extending from 2 to 4 eV. At x-ray photon energies the atomic cross section for the 3*d* bands is larger than the atomic cross section for 2*p* bands,[19] whereas the reverse is reported at the UV photon energies. Observations based on this simplistic argument would suggest that at higher photon energies the valence-band electron removal spectrum receive the main contribution from 3*d* bands, whereas at UV photon energies the main contribution is given by the 2*p* bands. However, it is important to note that the intensity of the valence-band electron removal spectrum is so far to be described by a pure atomic picture since the 2*p*-3*d* hybridization can introduce states with a strongly mixed character. In this light, the comparison between the features of valence-band electron removal spectra per-

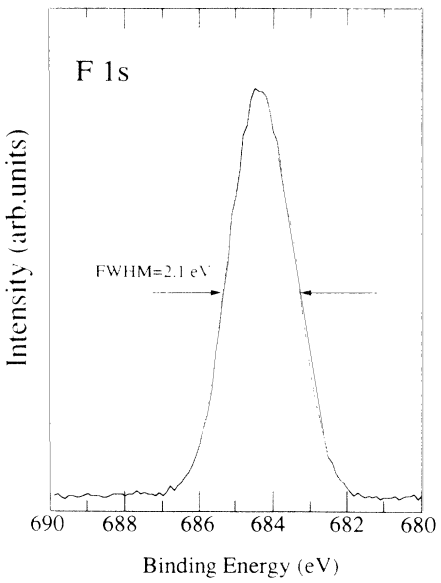

FIG. 1. F 1*s* core-level XP spectrum for K_2NiF_4.

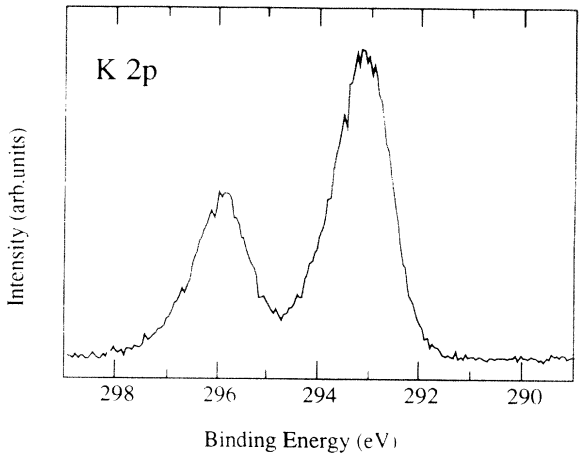

FIG. 3. K 2*p* core-level XP spectrum for K_2NiF_4.

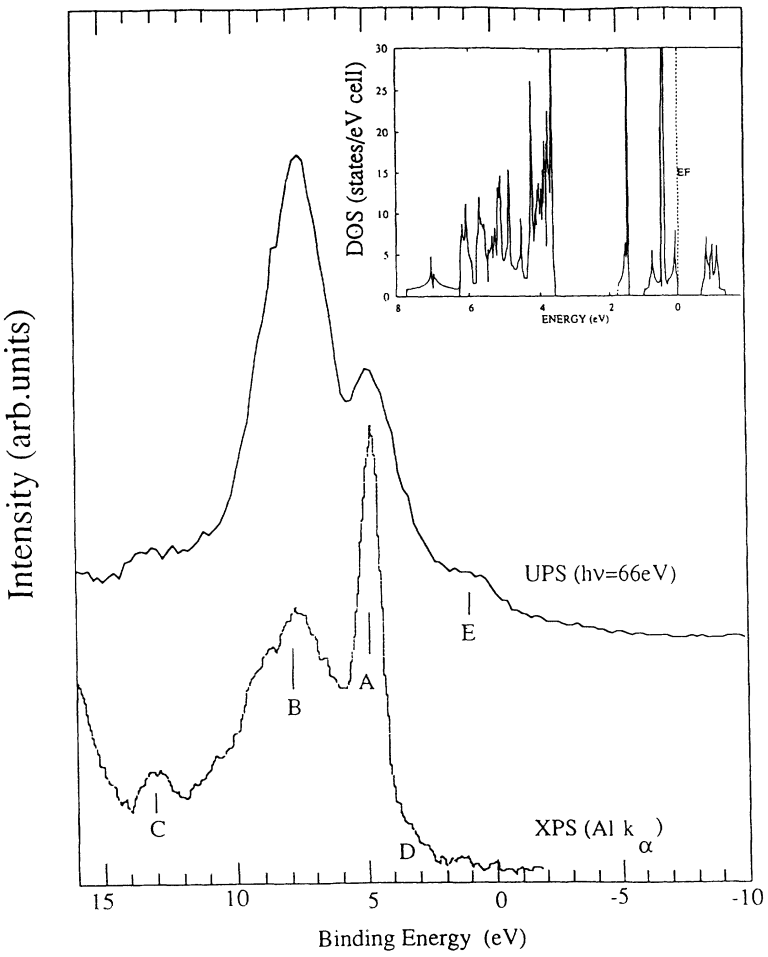

FIG. 4. Valence-band XP and UP spectra for K_2NiF_4. The main spectral features ($A-E$) discussed in the text are evidenced. Inset: calculated LDA spin-polarized density of states. The experimental energy is referred to the K $3p$ peak which has been set at 18.36 eV. The density-of-states energy zero is set at the calculated Fermi energy (EF), indicated by a vertical dashed line.

formed at different photon energies cannot be regarded as an unambiguous evidence of their character. Therefore, peak B could receive a significant intensity also from the Ni $3d$ states. The CI cluster calculation reported in Sec. IV B will be helpful to identify the Ni contribution along the whole valence-band spectral range.

The inset of Fig. 4 reports the calculated total density of states (DOS) for the antiferromagnetic structure using density-functional theory as described above. The states below about 3.5 eV are the F $2p$ states and the states from the Fermi energy (set at 0 eV) to about 2 eV are the Ni $3d$ states. The character of each of the two regions is attributed to one single atomic species (either Ni or F) since the hybridization between Ni and F orbitals determines only a minor contribution of Ni states in the region below 3.5 eV as well as of F states in the 0–2-eV region.

Though the experimental data exhibit significant discrepancies with LDA band-structure calculations, useful information about the degree of correlation could be obtained pointing out these discrepancies. As is well known, when one-electron band-structure calculations are used to describe highly correlated systems, some important features of the experimental spectra are missed. In particular, satellite structures due to many-body effects are not reproduced by such calculations. That is clearly observed also in the present case if the XPS and UPS valence-band spectra are compared with the LDA density of states shown in the inset of Fig. 4. On the contrary, since one-electron band-structure calculations satisfactorily reproduce band insulators with no correlation effects, such as Cu_2O,[20] this is turn demonstrates that when electron-correlation effects are present important features of the valence-band electron removal spectrum are missed by such calculations.

Other important, but less evident, differences between the experimental spectra and the LDA results are (1) the distance between the centroids of the Ni $3d$ and F $2p$ partial DOS from the LDA is somewhat larger than the energy separation of peak A and B; (2) the gap between Ni $3d$ and F $2p$ partial DOS is not visible in the XPS valence-band spectrum, contrary to the Cu_2O case (a band insulator showing no correlation effects) where such a gap between the Cu $3d$ and O $2p$ partial DOS can be observed both experimentally and theoretically;[20] (3) the experimental peaks A and D are not consistent with the line shape of the Ni $3d$ partial DOS between 0 and 2-eV energy. These issues will be discussed in Sec. IV B along with the impurity-cluster results.

Some details still remain to be clarified as regards the structures D and E appearing on the low BE side. The D structure in the XP spectrum, on the basis of a comparison with the calculated DOS, could be associated to

states lying at low BE (below 0.5 eV) in the DOS, even though the experimental separation from the main line is higher than the calculated separation. Model-Hamiltonian cluster calculations performed by van Elp, Eskes, and Sawatzky for Li-doped NiO (Ref. 21) attribute to the first ionization state a ^2E_g character. On the contrary, Fujimori and Minami,[22] using a different set of parameters and a point charge-crystal-field splitting of different sign and smaller magnitude, found that the first ionization state has $^4T_{1g}$ character. On this basis the present data peak *D*, because of its energy position and intensity, could be attributed to a low-intensity ^2E_g state. Nevertheless, calculations reported in the present paper for the NiF_6^{4-} cluster (see Sec. IV B), indicate that the first ionization state has a $^4T_{1g}$ character in spite of the fact that the crystal-field splitting has the same sign (Table I) as obtained by van Elp.[21]

In the UPS spectrum, a peak (*E*) appears at 1 eV. This peak has not a counterpart in the XPS spectrum. It could be attributed to the presence of surface states, resulting from the cleavage, whose contribution should be enhanced in the case of the more surface-sensitive UPS measurements. At the present, we are not able to unambiguously address the *E* structure assignment, so we will not discuss it in the following.

Figure 5 shows the UP spectra taken at photon energies of 66 eV and 60 eV. The spectra have been normalized with respect to the F 2*p* peak. The peak at 18.36 eV is attributed to K 3*p* levels. The most remarkable difference between the two spectra is the satellite structure *S*. This structure is clearly evident in the $h\nu=66$-eV data, but, in the $h\nu=60$ eV, it has disappeared. The photon energies chosen to acquire the spectra, corresponding to the cases of below-resonance (60 eV) and above-resonance (66 eV) energy, where the resonance energy is referred to the resonance across the Ni 3*p*-3*d* transition threshold.

TABLE I. Parameters values used for the XPS valence-band data fitting (all energies in eV units).

Energies (eV)	
δEA	8.5
δEB	0.5
δEC	7.0
$10Dq$	0.25
Δ	8.5
$(pd\sigma)$	−1.73
$(pd\pi)$	0.78
$(sd\sigma)$	−2.07
$(pp\sigma)$	0.54
$(pp\pi)$	−0.09
Racah parameters	
Ni^{2+}	$A=8.0$
	$B=0.127$
	$C=0.601$
Ni^{3+}	$B=0.138$
	$C=0.676$
$U(^4T_{1g})$	8.14

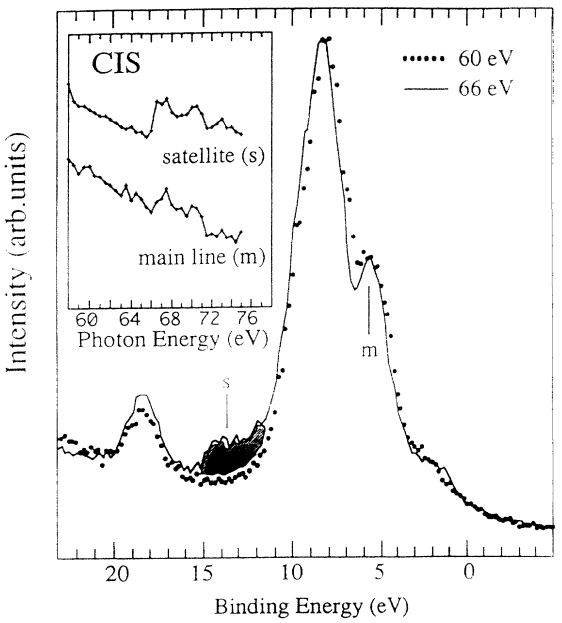

FIG. 5. UP spectra taken at $h\nu=60$-eV (dots) and 66-eV (full line) photon energy. The Ni main line (*m*) and the Ni satellite (*S*) are also indicated. Inset: CIS spectra relative to the main line (*m*) and to the satellite (*s*) initial energies.

Since peak *S* intensity increases passing through the resonance threshold, this experimental evidence strengthens the attribution of peak *S* to Ni 3*d*-electrons removal spectrum. Moreover, the CIS spectrum relative to the satellite (inset of Fig. 5), taken at a constant initial energy of 13.5 eV, shows a more evident resonance effect with respect to the main line CIS spectrum, taken at an

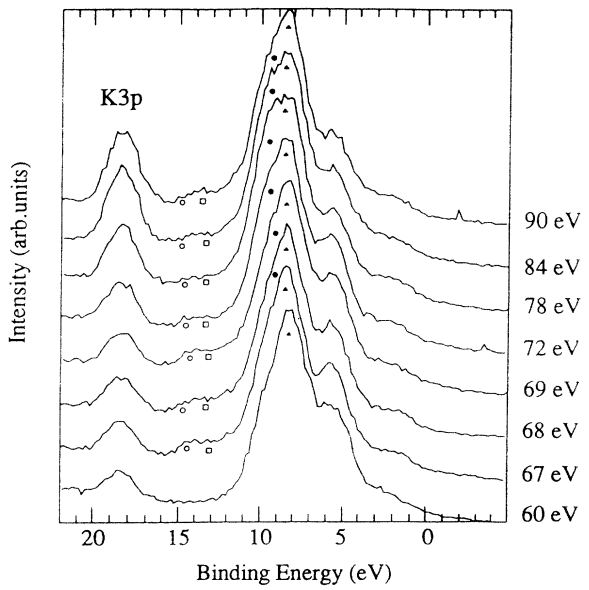

FIG. 6. Valence-band region UP spectra taken at different photon energies (from 60 to 90 eV) in a normal-emission configuration. The peak at 18.36 eV is the K 3*p* contribution.

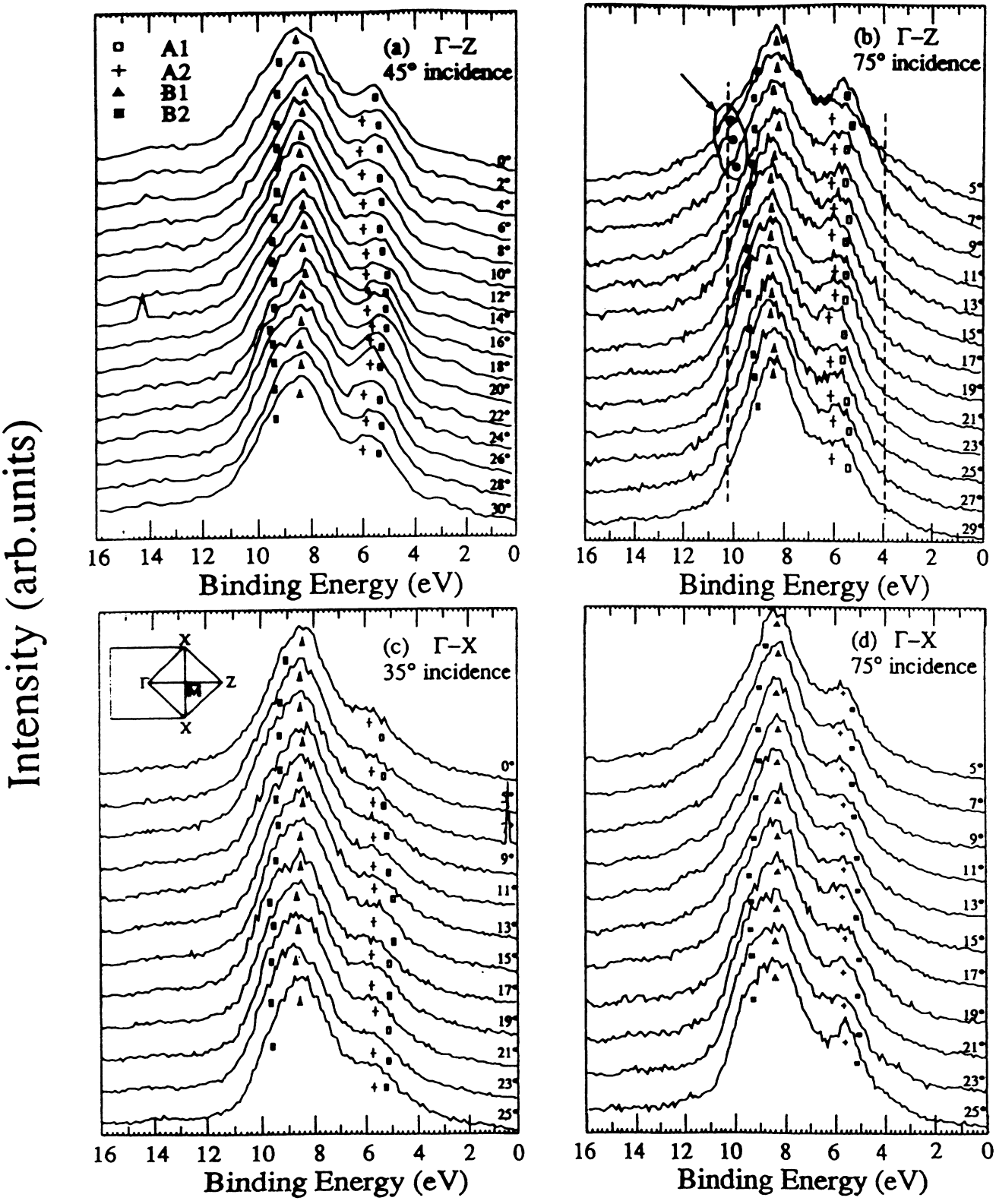

FIG. 7. Angle-resolved photoemission data of K_2NiF_4, taken at $h\nu = 66$-eV photon energy along the Γ-Z direction at 45° (a) and 75° (b) photon incident angle and along the Γ-X direction at 35° (c) and 75° (d) photon incident angle. The directions in the k space are reported in panel (c). Four slightly dispersing contributions have been evidenced. They are labeled as $A1$, $A2$, $B1$, and $B2$ in panel (a). In panel (b), two vertical lines and an arrow indicate spectral regions where a further, not resolved, contribution to the density of states might be seen.

initial energy of 5.6 eV.

However, the uncertainty involved in the normalization procedure of the on- and off-resonance spectra is quite large compared with the spectral enhancements at the 3*p* edge. For this reason, we do not feel confident in giving a quantitative interpretation of the difference in the resonance effect between the main line and the satellite.

Figure 6 reports the UPS spectra of valence band and K 3*p* core levels for different photon energies. The photoemitted electrons are collected in a direction normal to the sample surface (normal emission setup). This setup allows us to detect the band dispersion parallel to the crystallographic *c* direction. With the aim of pointing out the dispersion of the F 2*p* band, the spectra have been normalized to F 2*p* peak. As a consequence, the K 3*p* peak shows an intensity increase with the photon energy greater than the expected $\sigma_{K\ 3p}$ increase. The satellite at 13.5 eV appears structured, even if the experimental resolution does not allow us to evidence the details on a finer scale. The peak *B*, with a prevalent F character, shows a broadening when the photon energy is higher than 72 eV. This feature could be interpreted as a weak dispersion of the F 2*p* bands. Actually, since K_2NiF_4 has a layered structure, only a very small dispersion is expected to occur in the *c* direction.

Figures 7(a)–7(d) report the data obtained with a constant photon energy and a variable take-off angle (off-normal emission). The photon energy has been fixed at 66 eV, that is in the resonance conditions, in order to follow the metal bands dispersion more easily through an enhancement of their contribution to the spectrum. For each high-symmetry direction in the *k* space [Γ-*Z* or Γ-*X*, see inset of Fig. 7(c)], the data relative to near-normal (75°) and less-normal (35° or 45°) incidence are reported. Even though we did not detect any polarization effect, the choice of taking both near-normal and near-grazing incidence spectra is important to check the consistency of the data, since in this way it is possible to obtain two independent dispersion measurements in the same *k*-space direction.

In each spectrum, four structures have been identified. Two of them (*A*1 and *A*2) were found to contribute to the Ni main line in the range 5–6 eV, and two other structures (*B*1 and *B*2) were found to contribute to the F 2*p* peak in the range 8–9.5 eV. Even though not all the features can be seen at all time, due to continuity, we indicate them in every spectrum. The dashed lines at 10.5

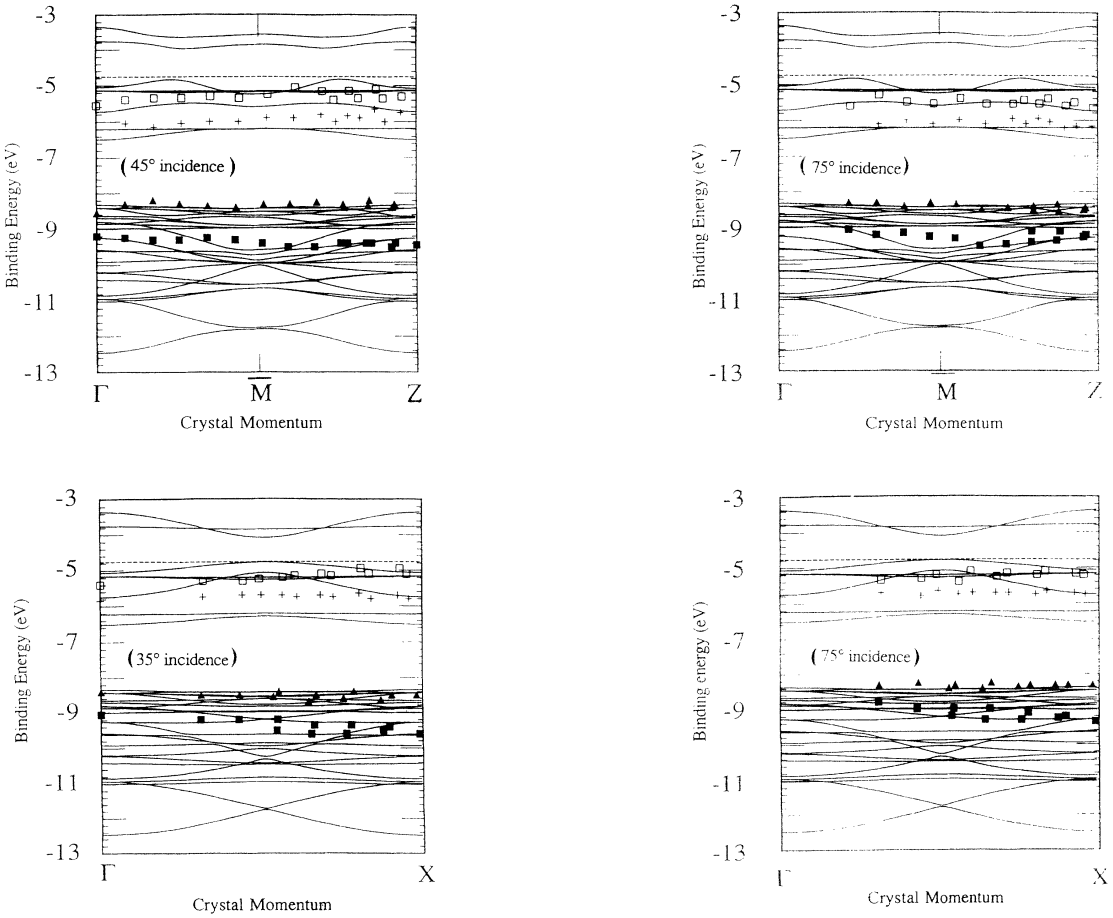

FIG. 8. Comparison of experimental *E* vs **k** relations with the spin-polarized LDA calculated bands. The calculated dispersion curves have been rigidly shifted to match the experimental curves. Dispersion curves along the Γ-*Z* direction at 45° (a) and 75° (b) photon incident angle and along the Γ-*X* direction at 35° (c) and 75° (d) photon incident angle are reported.

and 4 eV also indicate areas where it is possible to observe spectral components. Some of them are highlighted by an arrow [Fig. 7(b)].

Measured band dispersions are reported in Figs. 8(a), 8(b), 8(c), 8(d), superimposed to our calculated bands. The experimental values of $E(k_\parallel)$ have been calculated through the relation

$$k_\parallel = 0.51\ \text{Å}^{-1} \sin\theta \sqrt{E_{\text{kin}}(\text{eV})}\ , \tag{1}$$

where the electron kinetic energy E_{kin} and the emission angle θ are the experimentally measured quantities. The calculated bands have been rigidly shifted in energy to match the experimental data. This is necessary since a common energy zero in the calculation and experiment cannot be extracted.

The energy separation between the measured fluorine and the nickel bands is somewhat smaller than the separation resulting from the band-structure calculations. A puzzling aspect of the angle-resolved photoemission data in Figs. 6 and 7 is that they hardly disperse. In fact, in the case of the $B1$ band the measured dispersion is 0.5 eV at the most. Moreover, from a preliminary overview, the experimental dispersion of the bands—in particular, the F $2p$ bands—seems to be smaller than the theoretical one. This is puzzling because earlier ARPES work on NiO show very clear dispersion of several volts.[5] In addition, recent work on LiF by Himpsel *et al.*[23] also revealed large dispersion of 3.5 eV. This leads one to wonder whether this lack of dispersion is caused by materials problem at the surface or is due to interesting physics. Based on our experience, K_2NiF_4 is a harder material to work with than NiO. Cleavage plane is not as flat and the charging problem is much worse. Data in Figs. 6 and 7 should be regarded as the results of the best preliminary study of K_2NiF_4, given the intrinsic difficulties associated with photoemission from this material. More experiments are needed to check the data when better crystals or experimental conditions are available. We note, however, that if the F bands have had several eV dispersion (similar to NiO and LiF), then the charging problem will make the bands broader than what we observe. This argues against the sample charge as the sole problem for us.

The observed lack of dispersion can be interpreted in two ways. (i) Owing to the great number of bands (12) occurring in the valence-band region, we are not able to see the dispersion of individual bands; (ii) fluorine bands are less dispersed than the calculated bands. We argue that (i) is the more likely scenario and that it is similar to the case of high-T_c superconductors.

IV. DISCUSSION

A. Core-level data. Charge-transfer and Mott-Hubbard energies

Satellite structures in Ni $2p$ XP spectra of NiO and Ni halides are due to charge-transfer- and Mott-Hubbard-type charge fluctuations. To qualitatively investigate the effect of these correlations also in the case of K_2NiF_4, a fitting of Ni $2p$ core-level data using the CI impurity-cluster model previously applied to NiO and Ni halides[2,3] was performed. The XPS data fitting based on a configuration interaction of three states is only an approximation to the complex multiplet-split spectrum. Nevertheless, an estimate of CT and Hubbard correlation energies can be obtained. In particular, through the calculation of the average number $\langle n_{3d} \rangle$ of Ni $3d$ electrons in the ground state, useful information about the Ni-ligand bond ionicity can be obtained. The higher $\langle n_{3d} \rangle$ is, the less ionic the bond is.

The problem of photoemission from core levels has been treated by describing the photoemission process initial state as a system with eight d electrons (i.e., two d holes) and including the configuration $3d^9\underline{L}$ and $3d^{10}\underline{L}^2$, where $\underline{L}$ represents a p hole on the ligand. The final state of the process is a seven electron state described through a configuration interaction among the $\underline{2p}3d^8$, $\underline{2p}3d^9\underline{L}$, and $\underline{2p}3d^{10}\underline{L}^2$ states, where $\underline{2p}$ represents the Ni $2p$ hole.

The fitting results are reported in Fig. 9, where the calculated Ni $2p_{3/2}$ XP spectrum is superimposed to the background-subtracted experimental data. The parameter values are listed in Table II, where, in addition to our results, the parameter values for NiO and NiF_2 are reported from Ref. 3. Because of the same ligand, the NiF_2 results should be comparable to the perovskite results, while NiO is expected to give parameter values reflecting its less-ionic nature.

Indeed, going from O to F compounds, the charge-transfer energy Δ increases from 5.0 to 6.5 eV while the

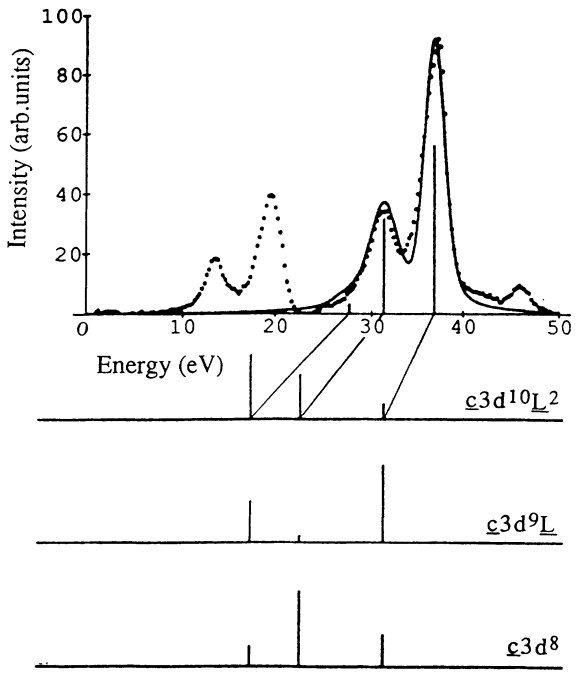

FIG. 9. Configuration-interaction impurity-model fitting results on Ni $2p_{3/2}$ core levels. Top: the calculated line shape (full line) is reported along with the experimental data (dots). The energies are in eV. Bottom: the relative weights of the three final-state configurations ($\underline{c}3d^8$,$\underline{c}3d^9\underline{L}$, and $\underline{c}3d^{10}\underline{L}^2$) are reported for each eigenvalue.

TABLE II. Ni 2*p* XPS data fitting results.

	Δ (eV)	U_{dd} (eV)	T (eV)	Q_{pd} (eV)	$\langle n_{3d} \rangle_{GS}$
NiO[a]	5.0	5.3	2.0	7.6	8.2
NiF_2[a]	6.5	5.0	2.0	7.0	8.14
K_2NiF_4	6.5	5.0	2.15	8.0	8.16

[a]Reference 30.

Mott-Hubbard U_{dd} repulsion is roughly constant (5.0–5.3 eV) since it refers to the same TM ion. Moreover, the ionicity increase is reflected by the decrease in the number, $\langle n_{3d} \rangle$, of 3*d* electrons in the ground state. In fact, $\langle n_{3d} \rangle = 8.2$ in NiO while $\langle n_{3d} \rangle = 8.16$ in K_2NiF_4 and $\langle n_{3d} \rangle = 8.14$ in NiF_2.

As it will be shown later, these results qualitatively match the valence-band results, even though different multiplet structures result from the core-hole photoemission ($\underline{2p}3d^8$) and from the valence-hole photoemission ($3d^7$) configurations. Moreover, since Δ, U_{dd}, Q, and T are effective parameters of the model Hamiltonians, the values obtained through core-level XPS data can be different from those obtained by valence-band data. However, being their physical meaning similar, the parameter trends should be similar.

A last remark should be done about the low-BE satellite-main-line intensity ratio, I_s/I_m. As one can observe comparing the NiO Ni 2*p* data[3] to the NiF_2 (Ref. 2) and K_2NiF_4 Ni 2*p* data, the Δ increase is followed by a decrease of I_s/I_m. This trend is also detectable comparing the NiO and K_2NiF_4 valence-band XP data and it will be used as a parameter constriction for the valence-band data fitting.

B. Angle-integrated valence-band data and configuration-interaction models

The experimental valence-band data show a remarkable satellite structure at 13.5 eV, similar to the one appearing in NiO (Ref. 22) and usually attributed to the effects of metal-metal, U_{dd}, and metal-ligand, Δ, charge fluctuations. In the following a detailed analysis of this issue is given to elucidate the discussion about the K_2NiF_4 band dispersion.

To compare calculated electronic structure to electron removal spectra obtained by photoelectron spectroscopies it is important to know of the final-state effects since it is not possible to directly compare the band structure, calculated for the *N*-electron neutral system, to the measured dispersion which refers to an excited state of the $N-1$ electron system. The problem of the comparison of calculated and experimental DOS is even more complex if the system studied presents strong correlation effects. The response of the system to the creation of a hole becomes apparent in the electron removal spectrum through peak asymmetries, satellite structures, and dispersions (i.e., bandwidth) variations. Some of these features can be observed not only in highly correlated systems, but also in simple metals such as Na and K, where correlation effects are already effective.[24,25]

The correlation effects characterizing the K_2NiF_4 electronic structure can be described within a configuration-interaction cluster model, as it has been done for HTSC's and for some TM compounds such as NiO.[22,26–31]

There exist different approaches to the calculation of the energy levels in the final state of the photoemission process. Among them, the more comprehensive are those proposed by Fujimori and Minami[22] and by Zaanen[31] and Van Elp[21,26] and applied to the study of NiO. As in the case of XP data, the problem of photoemission from valence levels has been treated describing the initial state through a configuration interaction among $3d^8$, $3d^9\underline{L}$, and $3d^{10}\underline{L}^2$ states, with $\underline{L}$ representing a *p* hole on the ligand. The final state of the process is a seven-electron state described through the $3d^7$, $3d^8\underline{L}$, and $3d^9\underline{L}^2$ configurations where Coulomb and exchange integrals have been fully accounted for on the basis of Sugano, Tanabe, and Kamimura[32] two-electron calculations.

Even if the three approaches, previously quoted, differ for the calculation method, the results on NiO show how the charge-transfer and the Mott-Hubbard charge fluctuations give a characteristic shape to the valence-band spectrum. The main behavior is the existence of a ~10 eV extended multiplet structure which overlaps the region where the O 2*p* spectral weight contribution is prevailing. A strong mixing between the final-state configurations, due to hybridization, is also observed. This fact gives a prevailing $3d^8\underline{L}$ character to the main line even if relevant contributions from $3d^7$ and $3d^9\underline{L}^2$ configurations are present. Similarly, the contribution of the charge-transfer $3d^8\underline{L}$ configuration to the satellite cannot be neglected.

The calculations of the origin of NiO valence-band spectral structures can be extended to K_2NiF_4. To this purpose, we applied the approach developed by Fujimori and Minami[22] for the study of NiO electronic structure to the analysis of K_2NiF_4 XP valence-band spectrum. The electronic ground state of Ni^{2+} in a cubic (O_h) crystal field is known to have a $t_{2g}^6e_g^2$ configuration with a $^3A_{2g}$ total symmetry. After *d*-electron photoemission from the $^3A_{2g}$ state, the final states have either $^4T_{1g}$, $^2T_{1g}$, or ^2E_g symmetry. For each symmetry, unscreened $3d^7$ and screened $3d^8\underline{L}$ and $3d^9\underline{LL}'$ configurations have been considered. Here, $\underline{L}$ and $\underline{L}'$ represent linear combinations of F 2*p* ligand orbitals, which have a π or a σ bonding with the Ni 3*d* bands, i.e., of t_{2g} and e_g symmetry, respectively. It is important to remark that the choice of the configurations involved in the description of both the initial and final state is not unique. Apart from the d^n and the charge-transfer screened $3d^n\underline{2p}$ configurations (where $\underline{2p}$ denotes a F 2*p* hole), other configurations can be introduced. They can be obtained from a linear combination of Ni 4*s* orbitals, of Ni 4*p* orbitals as well as of F 2*s* orbitals. Usually they lie high enough to be neglected and their screening effect can be treated as a renormalization of the effective parameters. However, in this paper, e_g-like molecular orbitals derived from F 2*s* orbitals have been added according to the procedure described by Fujimori and Minami and applied to the NiO and $NiCl_2$ cases.[22]

The initial-state wave function is formulated through a configuration interaction among the relevant states which describe the energetic of the photoemission process. Neglecting the multiplicity of the d^8-ion energy levels, the ground state can be written, in the most general form, as

$$\Psi_{GS}=a_0|d^8\rangle+a_1|d^9\underline{L}\rangle+a_2|d^{10}\underline{L}^2\rangle\ , \tag{2}$$

where the first term represents a state with eight d electrons (the unscreened Ni^{2+} ion) and the second term a charge-transfer state with a ligand hole. The term with double screening, $d^{10}\underline{L}^2$, lies at high energies with respect to the others and is sometimes neglected. In that case, the value of a_0 and a_1 can be found by diagonalizing the initial-state Hamiltonian, which has a general form:

$$\begin{vmatrix} E_8 & v \\ v & E_8+\delta E_A \end{vmatrix}\ , \tag{3}$$

where $E_8=\langle d^8|H|d^8\rangle$ and $\delta E_A=E(d^8\rightarrow d^9\underline{L})=\langle d^9\underline{L}|H|d^9\underline{L}\rangle-\langle d^8|H|d^8\rangle$ represents the energy required to move an electron from the ligand to the $3d$ metal orbitals and it is related to the charge-transfer energy Δ. The off-diagonal term $v=\langle d^8|H|d^9\underline{L}\rangle$ is the transfer integral for Ni $3d$-F $2p$ hybridization and it is written in terms of Slater-Koster[33] $(pd\sigma)$ and $(pd\pi)$ integrals.

For each final-state symmetry ($^4T_{1g}$, $^2T_{1g}$, and ^2E_g) the final-state Hamiltonian has the general form

$$\begin{vmatrix} E_7 & v' & 0 \\ v' & E_7+\delta E_B & v' \\ 0 & v' & E_7+\delta E_B+\delta E_C \end{vmatrix}\ , \tag{4}$$

where E_7 represents the energy of the d^7 state and it is dependent on the Racah parameters B and C; $\delta E_B=E(d^7\rightarrow d^8\underline{L})=\Delta-A$ represents the charge-transfer energy Δ from which the d-d Coulomb attraction energy, represented by the Racah parameter A, between a $3d$ electron and the $3d$ hole created by the photoemission is subtracted. This effect contributes to stabilize the $d^8\underline{L}$ states with respect to the d^7 states resulting in a different ordering of the final-state levels with respect to the initial-state levels. $\delta E_C=E(d^8\underline{L}\rightarrow d^9\underline{L}^2)$ is the energy required to transfer a second electron from the ligand bands to the $3d$ band and it is expected to include the U_{pp} ligand correlation energy. Also, in this case, the v' represent the hybridization energies which are symmetry dependent and can be written in terms of the Slater-Koster transfer integrals. In the full Hamiltonian, which has been built through 40 states (17 for the ^2E_g symmetry, 13 for the $^2T_{1g}$ symmetry, and 10 for the $^4T_{1g}$ symmetry),[22] we have included a point charge-crystal-field splitting ($10Dq$), which splits the $3d$ orbital energies in a triple degenerate t_{2g} level at $\varepsilon_d(t_{2g})=\varepsilon_d+4Dq$ and in a double degenerate e_g level at $\varepsilon_d(e_g)=\varepsilon_d-6Dq$. In the present case, $10Dq$ represents only the ionic contribution to the observed splitting of the crystal-field states which is measured through the energy separation between the ground state of the compound and the lowest-lying state associated to the intra-atomic d-d transitions. In the case of, e.g., NiO the energy of the first d-d optical transition ($^3A_{2g}\rightarrow{}^3T_{2g}$) has always been identified as the ligand field splitting between the $3d$ e_g and t_{2g} orbitals. This energy value is higher than the included point charge-crystal-field splitting as a result of the different hybridization contributions to the $^3A_{2g}$ ground state and $^3T_{2g}$ excited state.[21,22] Similar remarks hold for K_2NiF_4.[18] The value used for $10Dq$ in the case of K_2NiF_4 is 0.25 eV. It is somewhat lower than those used by Zaanen[31] ($10Dq=0.40$ eV) and by van Elp ($10Dq=0.70$ eV),[21] but it has the opposite sign with respect to the one used by Fujimori and Minami[22] ($10Dq=-0.5$ eV). The role of the crystal field has been considered also in defining the charge-transfer energy. In fact, the Slater-Koster[33] oxygen nearest-neighbor interactions $(pp\sigma)$ and $(pp\pi)$ split the oxygen states into a triple degenerate state with t_{2g} symmetry at the energy $\varepsilon_p(t_{2g})=\varepsilon_p-[(pp\sigma)-(pp\pi)]$ and into a double degenerate state with e_g symmetry at $\varepsilon_p(e_g)=\varepsilon_p+[(pp\sigma)-(pp\pi)]$. The value of $[(pp\sigma)-(pp\pi)]$ for K_2NiF_4, which is related to the F $2p$

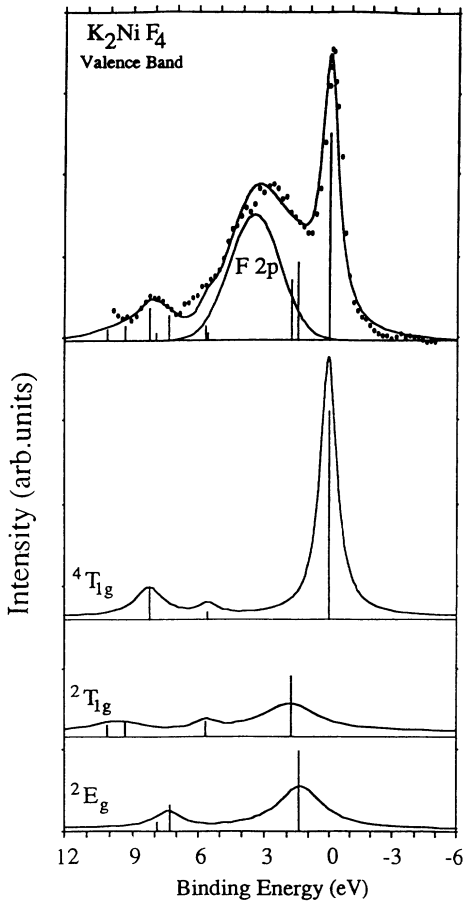

FIG. 10. The XPS valence-band spectrum (top, dotted line) of K_2NiF_4 compared to the configuration-interaction impurity-model calculation results (top, full line). The vertical bars indicate the position and the intensity of final states. The F $2p$ contribution is also indicated. In the bottom, the contributions of the different final-state symmetries ($^4T_{1g}$, $^2T_{1g}$, ^2E_g) to the total intensity are reported.

bandwidth, is 0.63 eV. Depending on the symmetry of the transferred electrons, the charge-transfer energy could be increased or decreased by an amount $[(pp\sigma)-(pp\pi)]$.

By using the same matrix elements and Racah parameters reported by Fujimori and Minami [Table I in Ref. 22], the energies and the contributions to the total intensity of the three final state symmetries were calculated. The results are reported in Fig. 10, Tables I and III. The parameter set was chosen to reproduce the main line to satellite intensity ratio as well as the main line to satellite energy separation. The value transfer integrals have been increased with respect to the corresponding values of NiO to account for the shorter Ni-ligand distance.

The fitting of the experimental data has been performed using δE_A, δE_B, and δE_C as free parameters. These values are related to the charge-transfer energy as well as to the *d-d* Coulomb interaction energy. In particular, the parameter δE_A is defined, in this work, as the energy required to move a charge from the ligand $2p$ levels to the metal $3d$ orbitals in the $^3A_{2g}$ ground state. Since the energies in (4) are referred to the lowest energy of the $^3A_{2g}$ multiplet, we set $\Delta=\delta E_A=8.5$ eV. This value is higher than the one obtained from a Ni $2p$ XP data fitting (Table II). This discrepancy can be attributed, in addition to the uncertainty in the parameter values (± 0.5 eV), to the fact that, in spite of the great number of configurations involved in the valence-band XP data fitting, in the Ni $2p$ XP data fitting Δ represents an average energy since only three configurations have been used to fit the data, neglecting all the multiplet-splitting effects. As a consequence of the higher values of Δ, also A and U_{dd} will result to be higher than in the $2p$ photoemission case.

The Hubbard energy can be calculated on the basis of Racah parameters. In our case, B and C are the free ion values, while A is related to the Coulomb two-electron integral F^0 ($A=F^0-F^4/9\sim F^0$). The value of A can be estimated from the values of Δ and δE_B through the relation $A=\Delta-\delta E_B=8.0$ eV. Finally, since in the case of $^4T_{1g}$ symmetry $U_{dd}=A+B$,[21] the Mott-Hubbard U_{dd} energy is 8.14 eV. These calculations represent only a preliminary result since they give a consistent deconvolution of the experimental data but further refinements are required to elucidate some important details concerning the symmetry of the lowest-lying (i.e., the first ionization) states.

TABLE III. Valence-band fitting results. Relative energies, intensities, and configuration weights of the ground state and of the low-BE ionization states.

Ground state			Ionization (final) states		
Γ	$^3A_{2g}$		$^4T_{1g}$	^2Eg	$^2T_{1g}$
		Relative BE (eV)	0.00	1.41	1.80
		Intensity (a.u.)	9.69	4.16	3.31
		Configuration weights (%)			
d^8	86.2	d^7	55.9	43.0	52.0
$d^9\underline{L}_p$	11.0	$d^8\underline{L}$	39.1	49.0	45.9
$d^9\underline{L}_s$	2.8	$d^9\underline{L}^2$	5.0	8.0	2.1
$\langle n_{3d}\rangle$	8.14	$\langle n_{3d}\rangle$	7.49	7.65	7.50

To investigate the character of the first ionization state, the energy of the ^2E_g and $^4T_{1g}$ states has been studied as a function of the charge transfer Δ, crystal field, and F $2p$-Ni $3d$ transfer integrals ($pd\sigma$) parameters in the O_h point group symmetry. Though the complete analysis of this issue will be reported elsewhere,[18] it can be anticipated that, upon a variation of Δ between 7.5 and 9.5 eV and $|(pd\sigma)|$ between 1.4 and 2.00 eV, $^4T_{1g}$ always remains the first ionization state. On the contrary, the level ordering is quite sensitive to the value of the crystal-field term, $10Dq$. In fact, for $10Dq\geq 2$ eV, the ^2E_g state attains the lowest binding energy. However, in this case the data fitting becomes questionable since the calculated intensity ratio between peak A and C and their energy separation become considerably different from the experimental values. In the light of this result, the character of the first ionization state for K_2NiF_4 seems to be different from that obtained by van Elp[21] in the case of NiO, i.e., $^4T_{1g}$ vs ^2E_g. The investigation of the first ionization state turned out to be crucial in the study of HTSC's and related compounds,[30] where the distortion from O_h to D_{4h} is crucial in stabilizing the $^1A_1$ Zhang-Rice singlet. To this connection it is important to recall that a possible tetgragonal distortion of K_2NiF_4 unit cell has been pointed out by Birgenau, Guggenheim, and Shirane.[7] A calculation including the effects of this distortion in the matrix elements could complete the analysis of the problem.

Going back to the fitting results reported in Fig. 10 and Table III, one can observe that the $3d$-electron spectrum is spread over a 10-eV range. The $^4T_{1g}$ state mainly contributes to the main-line intensity. Setting the $^4T_{1g}$ state energy as the reference (zero) energy, contributions from ^2E_g and $^2T_{1g}$ symmetry states can be found at 1.41 and 1.80 eV. The intensity of these structures is hardly detectable also in the XPS spectrum because of the relevant contributions coming from the F $2p$ electrons, which has been added to the calculated $3d$-electron spectrum as a Gaussian peaked at 3.45 eV from the main line. Nevertheless, a careful analysis of experimental XPS data (Fig. 4) suggests the possibility of finding a not negligible contribution to the spectral intensity between the main line A and the broad peak B, in spite of the broad gap between F $2p$ states and Ni $3d$ states predicted by the calculated DOS. Two low-intensity states with $^4T_{1g}$ and $^2T_{1g}$ symmetry, peaked at 5.50 and 5.65 eV, contribute to the region on the low BE of the satellite (C structure, Fig. 4) which results from the contribution of several peaks extending from 7.35 to 8.39 eV.

A quick review of the results relative to NiO (Refs. 21, 22, and 31) shows that the number of d electrons is close to, or slightly greater than, 8. For the perovskite, the higher ligand electronegativity produces a higher degree of ionicity. In particular, for the main line, the weight of the unscreened $3d^7$ configuration overcomes the weights of the $3d^8\underline{L}$ and $3d^9\underline{L}^2$ configurations in the case of $^4T_{1g}$

and $^2T_{1g}$ symmetries (Table III). This increase produces a prevailing $3d^7$ weight in the main line. The average number $\langle n_{3d} \rangle_{FS}$ (where FS is final state) of $3d$ electrons for the first three ionization states is 7.54.

The higher ligand ionicity is expected to open a wider gap between the Ni $3d$ bands and the ligand $2p$ bands. Comparing NiO (Ref. 22) to K_2NiF_4 data, one can observe that the energy separation between the centers of gravity of $2p$ and $3d$ bands is smaller than 2 eV in NiO while it is greater than 2.5 eV in K_2NiF_4.

Comparing Δ and U_{dd}, one can determine in which region of the Zaanen, Sawatzky, and Allen (ZSA) (Ref. 34) the classification scheme K_2NiF_3 should be placed. The U_{dd} value is determined with reference to the lowest free ion multiplet of d^7, d^8, and d^9 and results to be $U(^4T_{1g})=8.14$ eV. Compared with $\Delta=8.5$ eV, one is induced to place K_2NiF_4 in the intermediate region of the ZSA phase diagram.

C. Angle-resolved valence-band data and band-structure calculations

The picture of the photoemission process that we have drawn so far is useful to introduce a study where calculated band-structure and experimental results can be compared. One of the most interesting issues that can be discussed is the degree of approximation that a theoretical description of the N electron system can give of the experimental $N-1$ electron final state. Band-structure calculations that make use of a single Slater determinant of one-electron wave function can properly describe the electronic structure in the presence of electron-correlation effects only if the Mott-Hubbard Coulomb energy U_{dd} is negligible compared to the one-electron bandwidth. In this case, the electron-correlation many-body problem can be approximated to the one-electron problem and conventional band-structure calculations can be applied. In the presence of strong correlation effects the band structure calculated from one-electron wave function does not represent an acceptable approximation of the intrinsic electronic structure. Indeed, the comparison between the band structure obtained by photoemission experiment and calculated spectra can be done only if the photoemission spectra are obtained by calculating the projection of the N electron ground state with one-electron removed onto the $N-1$ state. The analysis through the configuration interaction cluster model allows us to point out that when the correlation effects are large, as in the case of K_2NiF_4, the transition-metal $3d$ spectral weight is spread on a wide energy range (10 eV, in the present case) with a significant intensity also in the high-binding-energy region (C structure, Fig. 4). This result represents a major discrepancy between the LDA results and the experiments. The LDA calculations miss a substantial amount of the $3d$ spectral weight in the high-energy region.

As it has been previously recalled, from a comparison of NiO (Ref. 22) with K_2NiF_4 data, one can observe that the energy separation between the centroid of F $2p$ and Ni $3d$ bands in NiO is smaller than in K_2NiF_4. This energy separation can be affected by the electronic correlations. Before switching on the hybridization between the d^7, $d^8\underline{L}$, and $d^9\underline{L}^2$ states, the $d^8\underline{L}$ and the $2p^5$ states have the same energy. Upon switching on the hybridization, states of primarily $^4T_{1g}$ character are formed out of the d^7, $d^8\underline{L}$, and $d^9\underline{L}^2$ states to produce peak A. The energy separation between peak A and B depends strongly on the details of the hybridization, i.e., the multiplet-dependent parameter values of Δ, U_{dd}, and $10Dq$ and on the $2p$-$3d$ and $2p$-$2p$ transfer integrals.

The degree of ionicity relative to the Ni-ligand bond remains the main difference between NiO and K_2NiF_4. Since the Ni-O bond has a lower degree of ionicity with respect to the Ni-F bond, NiO band structure is expected to show some Ni d bands very close to the oxygen bands. This is indeed what one can observe in NiO band dispersion measurements,[5] where a Ni band is located very close to an O band in the Γ point of Γ-X direction. The same features cannot be observed in K_2NiF_4 angle-resolved UP spectra, because of the high number of F $2p$ bands contributing to the valence-band spectral intensity. Nevertheless, few remarks can be done observing the angle-integrated valence-band fitting results. The superposition between a Ni band and an O band at Γ point in NiO has a counterpart in the impurity-cluster CI results. In fact, the energy separation ΔE between the $^2T_{1g}$ line and the ligand $2p$ bands center of gravity is smaller than 0.5 eV, as one can deduce from CI results,[22] while $\Delta E \cong 2.0$ eV in K_2NiF_4. For this reason, even if we are not able to resolve the band located in the region between A and B peaks in Fig. 4, we argue that Ni and F bands in K_2NiF_4 are well separated from each other.

V. CONCLUSIONS

An experimental and theoretical study of the electronic structure and correlations effects of K_2NiF_4 is presented. The Ni $2p$ XPS core lines as well as the valence-band electron removal spectra present the characteristic features of highly correlated systems. These data, analyzed through a configuration-interaction impurity-cluster model, allow us to estimate the charge fluctuation parameters, while their effects on the electron removal spectra are identified.

Angle-resolved photoemission experiments performed using a photon energy tunable source show a small dispersion of the bands. To tentatively describe the band-structure features of this compound, LDA calculations are used. Unfortunately, due to the high degree of correlation present in this compound, substantial discrepancies emerged between the experimental and the calculated DOS. In particular, the distance between the centroid of the Ni-$3d$ and F-$2p$ calculated partial DOS is larger than the separation between the two main components observed in the electron removal spectra, the gap present in the calculated Ni-$3d$ and F-$2p$ partial DOS is not visible in the XPS valence-band spectrum, the line shape of the Ni-$3d$ partial DOS is not consistent with that experimentally observed and, finally, the intensity distribution of the states observed in the electron removal spectra is substantially different from the calculated one.

These facts strongly indicate that the electron-

correlation effects are important and standard LDA calculation cannot be used to describe properly the band structure of narrow-band materials. On the other hand, it is important to suggest that one-electron parameters can be extracted from the LDA results and used for the many-body model Hamiltonian in order to reduce the number of parameters used to reproduce the experimental data.

Another important result arises when the present data and analysis are compared with those obtained on NiO. In particular, K_2NiF_4 presents quite reduced band dispersion with respect to NiO, which is not fully understood as well as the character of the first ionization state whose symmetry is found to be $^4T_{1g}$ instead of the ^2E_g symmetry found in NiO by van Elp and co-workers.

Furthermore, a comparison with results on NiO evidences the effect of the ligand electronegativity on the electronic structure. The experimentally measured energy separation between Ni and F bands is higher than the energy separation of Ni and O bands in NiO. This is an indication of the higher degree of ionicity of the Ni-F bond with respect to the Ni-O bond.

[1]G. van der Laan, C. Westra, C. Haas, and G. A. Swawatzky, Phys. Rev. B **23**, 4369 (1981).

[2]J. Zaanen, C. Westra, and G. A. Sawatzky, Phys. Rev. B **33**, 8060 (1986).

[3]G. Lee and S.-J. Oh, Phys. Rev. B **43**, 14 674 (1991).

[4]Jaehoon Park, Seungoh Ryu, Moon-sup Han, and S.-J. Oh, Phys. Rev. B **37**, 10 867 (1988).

[5]Z.-X. Shen, R. S. List, D. S. Dessau, B. O. Wells, O. Jepsen, A. J. Arko, R. Barttlet, C. K. Shih, F. Parmigiani, J. C. Huang, and P. A. P. Lindberg, Phys. Rev. B **44**, 3604 (1991).

[6]Z.-X. Shen, J. W. Allen, P. A. P. Lindberg, D. S. Dessau, B. O. Wells, A. Borg, W. Ellis, J. S. Kang, S.-J. Oh, I. Lindau, and W. E. Spicer, Phys. Rev. B **42**, 1817 (1990).

[7] R. J. Birgenau, H. J. Guggenheim, and G. Shirane, Phys. Rev. B **1**, 2211 (1970).

[8]J.-P. Gosso, P. Moch, M. Quilichini, J.-Y. Gesland, and J. Nouet, J. Phys. **40**, 1067 (1979).

[9]H. Sontag, F. Macco, K. Fendler, W. P. Lehmann, and R. Weber, J. Phys. C **15**, L409 (1982).

[10]K. Strobel and R. Geick, J. Phys. C **15**, 2105 (1982).

[11]G. Samoggia, F. Parmigiani, and F. Leccabue, Solid State Commun. **55**, 157 (1985).

[12]L. F. Mattheiss, Phys. Rev. B **5**, 290 (1972).

[13]K. Terakura, T. Oguchi, A. R. Williams, and J. Kubler, Phys. Rev. B **30**, 4734 (1984).

[14]R. Courths and S. Hüfner, Phys. Rep. **112**, 53 (1984).

[15]U. von Barth and L. Hedin, J. Phys. C **5**, 1629 (1972).

[16]O. K. Andersen, Phys. Rev. B **12**, 3060 (1975).

[17]O. K. Andersen, O. Jepsen, and D. Glötzel, in *Highlights of Condensed Matter Physics,* Proceedings of the International School of Physics "Enrico Fermi," Course XCIX, Varenna, 1984, edited by F. Bassani, F. Fumi, and M. P. Tosi (North-Holland, Amsterdam, 1985).

[18]L. Sangaletti, F. Parmigiani, and O. Jepsen (unpublished). After the present work was completed another density-functional electronic-structure calculation has appeared, i.e., V. Eyert and K.-H. Hoeck, J. Phys. Condens. Matter **5**, 2987 (1993).

[19]J. J. Yeh and I. Lindau, At. Data Nucl. Data Tables **32**, 1 (1985).

[20]J. Ghijsen, L. H. Tjeng, J. van Elp, H. Eskes, J. Westerink, G. A. Sawatzky, and M. T. Czyzyk, Phys. Rev. B **38**, 11 322 (1988).

[21]J. van Elp, H. Eskes, and G. A. Sawatzky, Phys. Rev. B **45**, 1612 (1992).

[22]A. Fujimori and F. Minami, Phys. Rev. B **30**, 957 (1984).

[23]F. J. Himpsel, L. J. Terminello, D. A. Lapiani-Smith, E. A. Eklund, and J. J. Barton, Phys. Rev. Lett. **68**, 3611 (1992).

[24]In-Whan Lyo and E. Plummer, Phys. Rev. Lett. **60**, 1558 (1988).

[25]M. M. Steiner, R. C. Albers, and L. J. Sham, Phys. Rev. B **45**, 13 272 (1992).

[26]A cluster model calculation of CoO, MnO, and Li-doped NiO valence-band photoemission spectrum is reported in J. van Elp, Ph.D. thesis, University of Groningen, 1991, Chaps. 3–5.

[27]A. Fujimori, M. Saeki, N. Kimizuka, M. Taniguchi, and S. Suga, Phys. Rev. B **34**, 7318 (1986).

[28]A. Fujimori, N. Kimizuka, T. Akahane, T. Chiba, S. Kimura, F. Minami, K. Siratori, M. Taniguchi, S. Ogawa, and S. Suga, Phys. Rev. B **42**, 7580 (1990).

[29]A. Fujimori, in *Core-Level Spectroscopy in Condensed Systems,* edited by J. Kanamori and A. Kotani (Springer-Verlag, Berlin, 1987), p. 136.

[30]H. Eskes, L. H. Tjeng, and G. A. Sawatzky, Phys. Rev. B **41**, 288 (1990).

[31]J. Zaanen, Ph.D. thesis, University of Groningen, 1986, Chap. 8.

[32]S. Sugano, Y. Tanabe, and H. Kamimura, *Multiplets of Transition-Metal Ions in Crystals* (Academic, New York, 1970).

[33]J. C. Slater and G. F. Koster, Phys. Rev. **94**, 1498 (1954).

[34]J. Zaanen, G. A. Sawatzky, and J. W. Allen, Phys. Rev. Lett. **55**, 418 (1985).

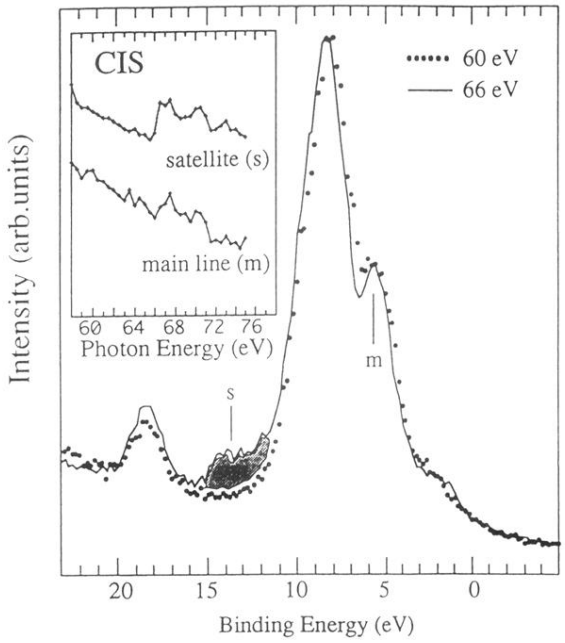

FIG. 5. UP spectra taken at $h\nu = 60$-eV (dots) and 66-eV (full line) photon energy. The Ni main line (m) and the Ni satellite (S) are also indicated. Inset: CIS spectra relative to the main line (m) and to the satellite (s) initial energies.